Journal of the European Ceramic Society 45 (2025) 117095

Contents lists available at ScienceDirect

Journal of the European Ceramic Society

journal homepage: www.elsevier.com/locate/jeurceramsoc

Ultrafast pressure sintering: A one-step route to dense high-entropy carbide from precursors

Xiang-Yu Bai, Yu Sun, Zhi-Yuan Cheng, Ping Shen *

Key Laboratory of Automobile Materials (Ministry of Education), School of Materials Science and Engineering, Jilin University, No. 5988 Renmin Street, Changchun 130025, PR China

ARTICLE INFO

Keywords:
High-entropy ceramics
Sintering
Densification
Ultrafast pressure sintering

ABSTRACT

Bulk high-entropy carbide ceramics (HECs) possess exceptional properties, but their fabrication typically involves energy-intensive and complex processes. This study introduces a novel ultrafast pressure sintering (UPS) method for the one-step synthesis and densification of HECs. Utilizing a custom-designed apparatus, this approach leverages the synergistic effects of direct Joule heating, reaction-released heat, and precisely controlled pressure to fabricate dense, single-phase, and homogeneous $(Cr_{0.2}Nb_{0.2}Ta_{0.2}Mo_{0.2}W_{0.2})C_{0.83}$ HEC with a fine-grained microstructure at a relatively low temperature of 1800 °C and a short dwell time of 3 min. Compared to conventional techniques such as hot-pressing and spark plasma sintering, UPS offers significant advantages, including reduced energy consumption, simplified processing, lower equipment costs, and enhanced scalability. This novel approach not only presents a promising route for the efficient fabrication of HECs, but also elucidates the underlying mechanisms governing their synthesis and densification, opening the way for broader applications in the development of advanced materials.

1. Introduction

High-entropy carbide ceramics (HECs) have attracted considerable interest due to their exceptional properties, including high melting points, hardness, and chemical stability, making them promising candidates for demanding applications in areas such as aerospace, gas turbines, and cutting tools [1–3]. However, widespread adoption and further development of HECs are currently hampered by the limitations of existing fabrication techniques, particularly the energy-intensive and complex nature of conventional high-temperature, high-pressure sintering.

Traditional HEC fabrication often relies on methods like hot-pressing (HP) or spark plasma sintering (SPS), typically involving separate stages for powder synthesis and densification. For example, Wang et al. [4] synthesized (TiZrNbTaMo)C high-entropy ceramics via a two-step carbothermal reduction and solid-solution method, a process requiring prolonged high-temperature dwelling and multiple intricate processing steps. While Wei et al. [5] employed SPS to shorten sintering times, the high equipment cost and substantial power requirements limit its scalability for mass production.

A groundbreaking ultrafast high-temperature sintering (UHS) technique was introduced by Hu et al. [6] in 2020. This method utilizes Joule heating generated by an electric current passing through carbon felt or graphite paper to rapidly heat the samples wrapped within, achieving significant advancements in the densification of oxide ceramics within remarkably short durations. Our previous research has successfully broadened the application of UHS to various non-oxide ceramics, demonstrating its potential for accelerated heating rates, reduced sintering times, and lower energy consumption [7–9]. However, the inherent softness of the carbon felt or graphite paper used in current UHS setups restricts the application of pressure during sintering, limiting its effectiveness in densifying certain refractory ceramic materials.

To address this limitation, we propose a novel ultrafast pressure sintering (UPS) method for the one-step synthesis and densification of HECs. This approach enables the simultaneous synthesis and densification of $(Cr_{0.2}Nb_{0.2}Ta_{0.2}Mo_{0.2}W_{0.2})C_{0.85}$ HEC at a relatively low temperature (1800 °C) within a short processing time of 3 min. Compared to the methods employed by Wang et al. [4] and Wei et al. [5], UPS not only reduces the sintering temperature and overall processing time (completing the entire process from heating to cooling within 15 min) but also significantly lowers energy consumption and simplifies the

---

* Corresponding author.
E-mail address: shenping@jlu.edu.cn (P. Shen).

https://doi.org/10.1016/j.jeurceramsoc.2024.117095
Received 6 August 2024; Received in revised form 3 November 2024; Accepted 19 November 2024

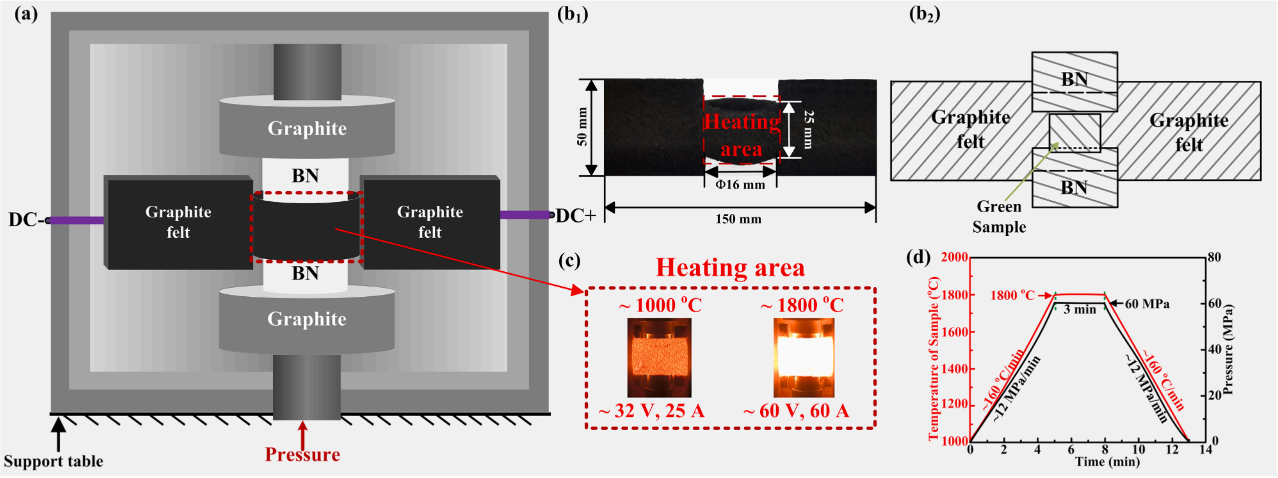

Fig. 1. (a) Schematic diagram of the custom-designed ultrafast pressure sintering (UPS) apparatus; (b$_1$) Structure and sizes of the carbon felt; (b$_2$) The relative positions of graphite felt, BN die, and sample; (c) Real-time images of sintering process; (d) Typical temperature and pressure curves.

fabrication process. Moreover, the simplicity and cost-effectiveness of the UPS equipment open new avenues for scalable production and broader application of HECs. This study further investigates the influence of temperature on phase evolution and compositional homogeneity, as well as the effects of pressure application timing and magnitude on densification, providing valuable insights into the underlying mechanisms governing the synthesis and densification of HECs.

2. Materials and methods

Dense $(Cr_{0.2}Nb_{0.2}Ta_{0.2}Mo_{0.2}W_{0.2})C_{0.85}$ (nominal composition) HEC was fabricated as a representative example to demonstrate the UPS process. High-purity oxide and carbon precursors were used for synthesis, including chromium oxide (Cr_2O_3, 99.9 %, 500 nm), niobium oxide (Nb_2O_5, 99.9 %, 200 nm), tantalum oxide (Ta_2O_5, 99.9 %, 200 nm), molybdenum oxide (MoO_2, 99.9 %, 50 nm), tungsten oxide (WO_3, 99.9 %, 50 nm), and graphite powder (C, 500 nm), all purchased from Shanghai Naiou Nanotechnology Co., Ltd., China. The carbothermal reduction reaction is represented by the following equation:

$$Cr_2O_3 + Nb_2O_5 + Ta_2O_5 + 2MoO_2 + 2WO_3 + 31.5\ C = 10\ (Cr_{0.2}Nb_{0.2}Ta_{0.2}Mo_{0.2}W_{0.2})C_{0.85} + 23CO \quad (1)$$

Stoichiometric amounts of the precursors were weighed and ball-milled for 60 min in a three-dimensional high-speed swing ball mill apparatus (MSK-SFM-3; Hefei Kejing Materials Technology Co. Ltd) using tungsten carbide balls and a milling jar. The resulting powder was then cold-pressed into cylindrical green compacts (8 mm diameter × 6 mm height) under a uniaxial pressure of 400 MPa.

One-step synthesis and densification were conducted in a custom-designed ultrafast pressure sintering furnace, as illustrated in Fig. 1(a). A piece of graphite felt, cut into the shape shown in Fig. 1(b$_1$), was symmetrically divided at its center to form an open cylindrical cavity with an approximate diameter of 16 mm and a length of 25 mm. This thin-walled cylindrical cavity generates concentrated Joule heat after being energized to heat the sample. The graphite felt was fixed between two copper electrodes. A green compact was placed in the central locating groove of the lower BN die (15 mm diameter), which was lined with 0.1 mm thick graphite paper to prevent sample adhesion. The lower BN punch was adjusted to extend into the cylindrical cavity of the graphite felt. The upper BN die was positioned approximately 1 mm above the green compact to ensure close contact between the BN die and the graphite felt. The relative positions of the graphite felt, BN die, and sample are shown in Fig. 1(b$_2$). In this setup, the graphite felt acted solely as the heating element, while the BN die assembly served as a pressurizing component. After evacuating the furnace chamber to approximately 5 Pa, a direct current (DC) was applied to the graphite felt, causing the cylindrical cavity at its center to rapidly heat up, thereby facilitating Joule heating.

The temperature was ramped at a rate of 150–300 °C/min, while pressure was applied at 10–15 MPa/min. The typical UPS process is

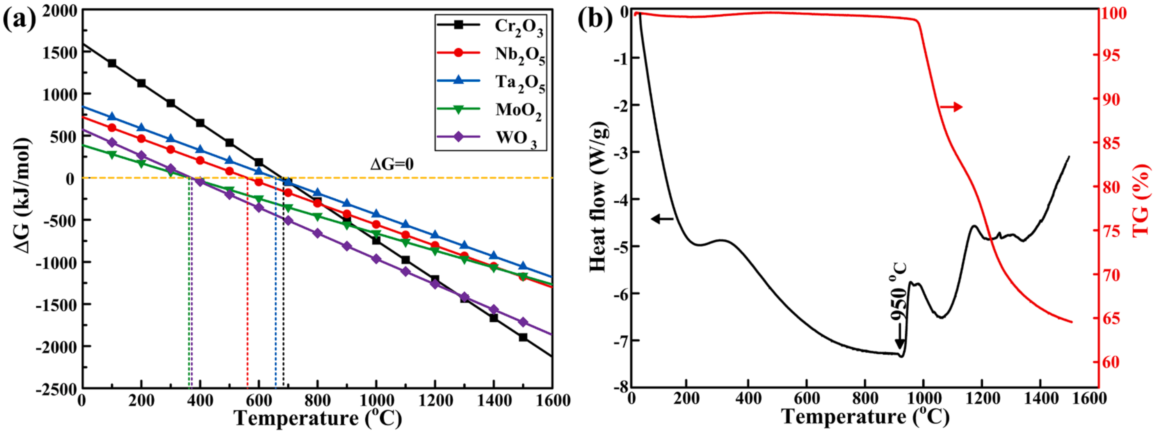

Fig. 2. (a) Relationship between the change in Gibbs free energy (ΔG) and temperature for the carbothermal reduction reactions of five oxides under vacuum (5 Pa); (b) DSC and TG curves of the green compact heated at a rate of 30 °C/min in an Ar atmosphere.

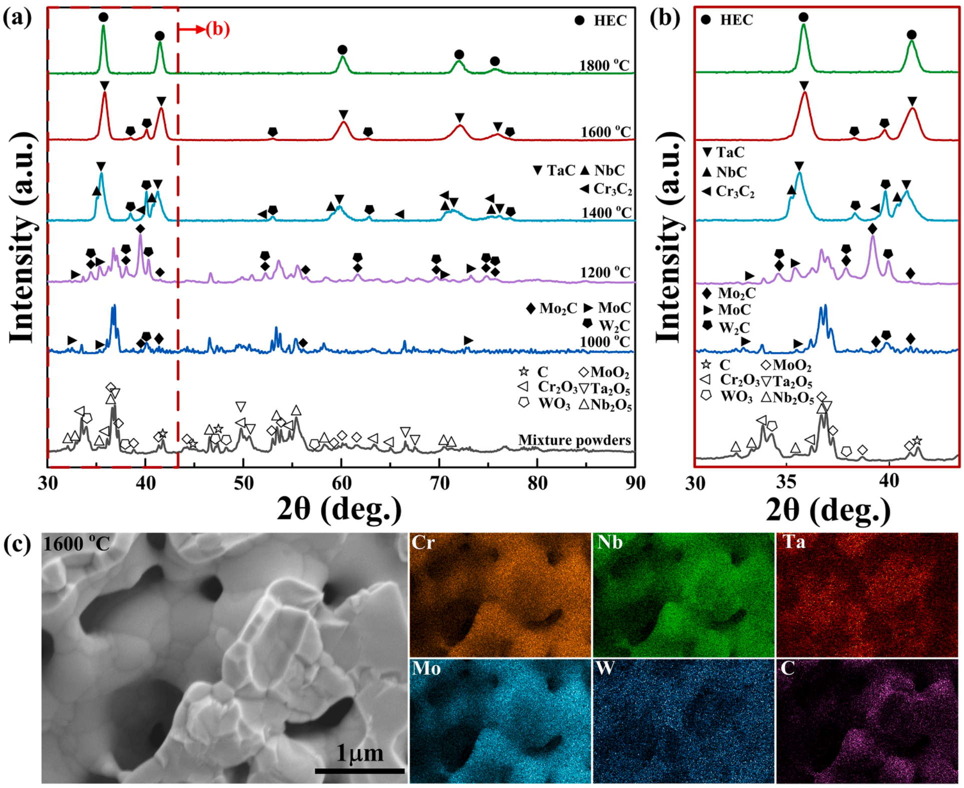

Fig. 3. (a, b) XRD patterns of samples held at different sintering temperatures under 60 MPa for 3 min; (c) SEM image and elemental mappings of the fracture surface of the sample obtained by UPS (1600 °C/60 MPa/3 min).

illustrated in Fig. 1(c). The temperature and pressure profiles under the optimized sintering parameters are shown in Fig. 1(d). The graphite felt surface temperature was monitored using an infrared thermometer (E1RH, Fluke, USA). The sample surface temperature was corrected according to the method described in the supplementary material of our previous study [10], with a temperature error of ±50 °C. All reported temperatures are the corrected values.

Differential scanning calorimetry (DSC, STA-449F5, NETZSCH, Germany) was used to determine the reaction temperature and weight loss of the green compact during heating. Phase composition and crystal structure of the sintered samples were characterized by X-ray diffraction (XRD, D/Max 2500PC, Rigaku, Japan). Density was measured using the Archimedes method, and relative density was calculated. Pore morphology was observed using optical microscopy (OM, Axio Imager

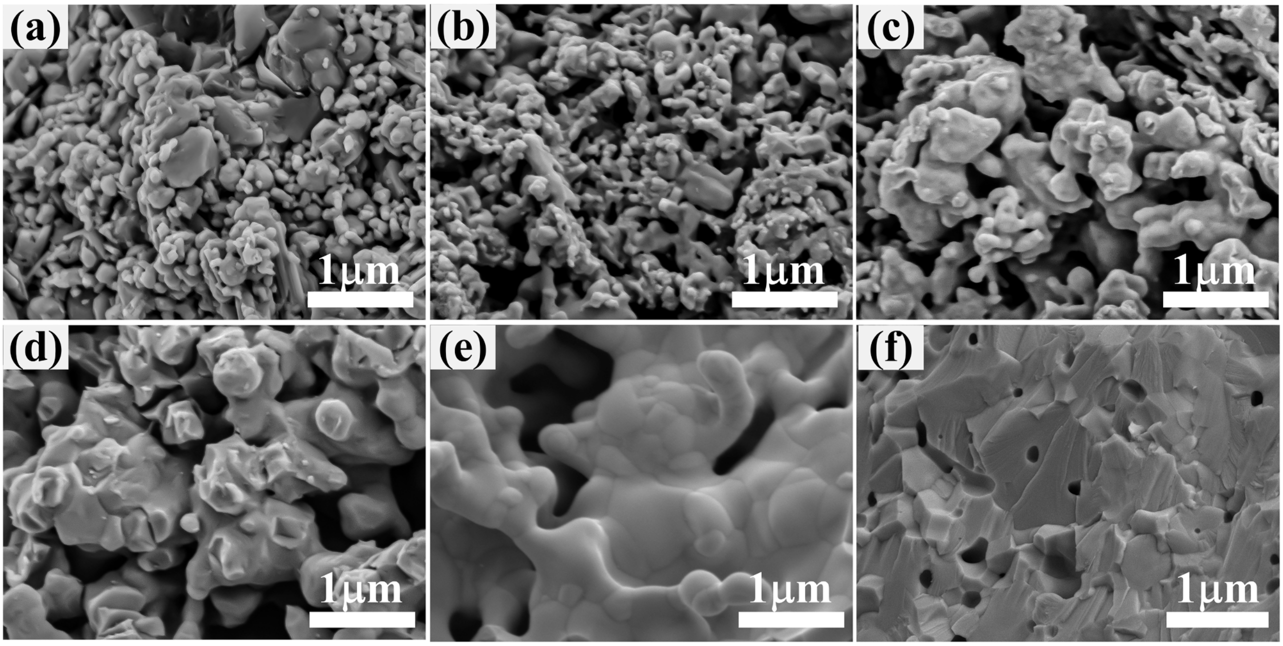

Fig. 4. SEM images of sample fracture surfaces under different UPS conditions: (a) Original compact; (b) 1000 °C/60 MPa/3 min; (c) 1200 °C/60 MPa/3 min; (d) 1400 °C/60 MPa/3 min; (e) 1600 °C/60 MPa/3 min; (f) 1800 °C/60 MPa/3 min.

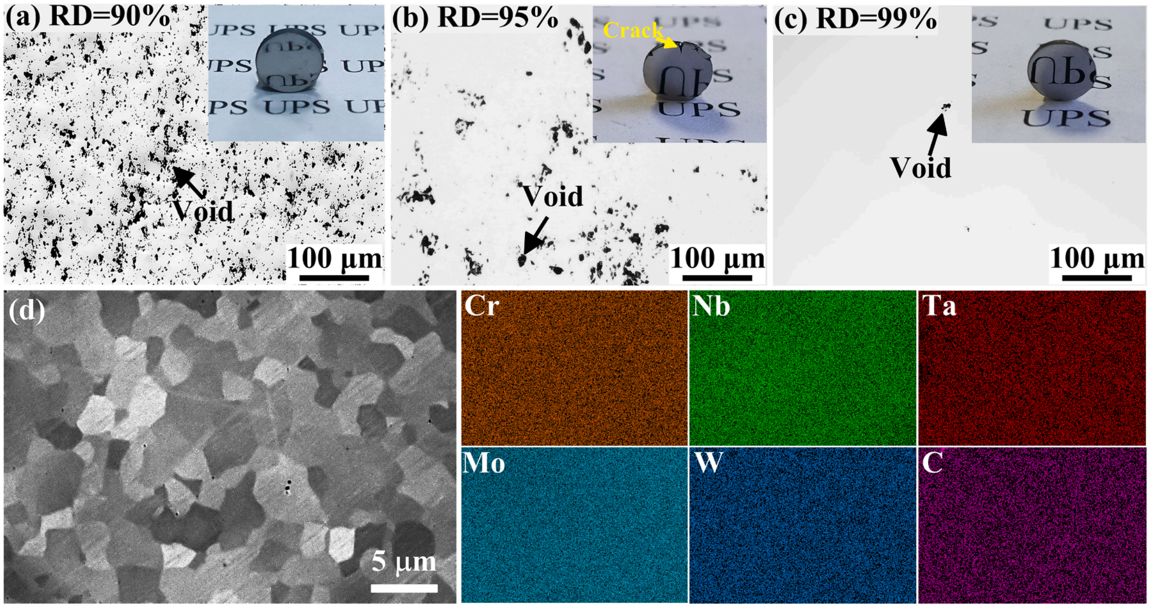

Fig. 5. Surface pore morphologies and macroscopic images of samples obtained at three different timings for pressure application (1800 °C/60 MPa/3 min): (a) Pressure applied after the carbothermal reduction reaction (~1400 °C); (b) Pressure applied before the carbothermal reduction reaction (~800 °C); (c) Pressure applied during the carbothermal reduction reaction (~1000 °C); (d) SEM image and elemental mappings of the sample in (c) (RD in the figures represents relative density).

A2m, Zeiss, Germany). Microstructural analysis was performed using field emission scanning electron microscopy (FESEM, JSM-7900F, JEOL, Japan) and transmission electron microscopy (TEM, JEM-2100F, JEOL, Japan) equipped with energy-dispersive X-ray spectroscopy (EDS). The carbon content of the sample was measured using a carbon/sulfur analyzer (CS744, LECO, USA). Vickers hardness of the dense samples was measured using a Vickers hardness tester (HVS-1000A, HuaYin, Hangzhou, China) under a load of 9.8 N and a dwell time of 10 s. Nanohardness and elastic modulus were determined using nanoindentation (G200, KLA-Tencor, USA) with a diamond Berkovich tip.

3. Results and discussion

To determine the critical temperature and reaction sequence of the carbothermal reduction, thermodynamic calculations were performed using the FactSage 8.3 software. The Gibbs free energy change (ΔG) for the five oxide-carbon systems under vacuum (5 Pa) is shown in Fig. 2(a). As anticipated, ΔG decreases with increasing temperature, indicating that the reaction becomes thermodynamically favorable when $\Delta G < 0$. The predicted critical temperatures for each individual oxide reduction, listed in Table S1, suggest a reaction sequence of $MoO_2 > WO_3 > Nb_2O_5 > Ta_2O_5 > Cr_2O_3$. However, it is important to note that the actual reaction pathway and kinetics are influenced by factors beyond thermodynamics, such as diffusion limitations and particle size. Differential scanning calorimetry (DSC) and thermogravimetric analysis (TG) of the green compact during continuous heating (Fig. 2(b)) reveal significant weight loss and an exothermic peak at 950 °C, indicating the onset of the carbothermal reduction reaction, which is accompanied by the release of carbon monoxide gas. As temperature increases, the continuous weight loss of the sample further reflects the progression of this reaction.

Guided by the DSC results, isothermal, isobaric (60 MPa, 3 min dwell time) UPS experiments were conducted starting at 1000 °C to analyze the phase evolution during sintering. Fig. 3(a–b) show the formation of Mo_2C, MoC, and W_2C between 1000 °C and 1200 °C. At 1400 °C, TaC, NbC, and Cr_3C_2 peaks emerged with the disappearance of all oxide peaks, indicating the completion of the carbothermal reduction. The broad TaC peak suggests the dissolution of Cr and Mo atoms into the TaC lattice, corroborated by the absence of distinct Cr_3C_2 and Mo_2C/MoC peaks, implying simultaneous reduction and solid-solution formation.

With increasing sintering temperature, the metal carbides progressively formed a single-phase $(Cr_{0.2}Nb_{0.2}Ta_{0.2}Mo_{0.2}W_{0.2})C_{0.85}$ HEC with a face-centered cubic (FCC) rock-salt structure through interdiffusion. The diffusion rate of the metallic constituents is crucial for the formation of high-entropy phase. In this system, TaC or NbC, with their larger lattice parameters [11], likely serves as the host lattice for the diffusion of Cr, Mo, and W [12,13]. The XRD patterns from 1400 °C to 1600 °C (Fig. 3(a–b)) suggest that Nb diffusion precedes W diffusion. Moreover, EDS mapping of the 1600 °C-sintered sample (Fig. 3(c)) shows that Cr, Mo, and Nb achieve solid solution before W. Considering the atomic radii of the metallic elements (Table S2), the diffusion rates are inferred to be Cr > Mo > Nb > W > Ta.

Microstructural evolution during UPS experiments (60 MPa, 3 min dwell time) at various temperatures (Fig. 4(a–f)) reveals a significant transition from loose powder to a dense structure between 1000 °C and 1800 °C. Neck formation and localized agglomeration are observed at 1200 °C (Fig. 4(c)), followed by increased particle bonding and the emergence of faceted grains at 1400 °C (Fig. 4(d)). At 1600 °C, grain growth leads to a continuous network with well-defined grain boundaries and rounded pores (Fig. 4(e)). Finally, at 1800 °C, significant pore reduction and strong intergranular bonding are observed, with the fracture mode transitioning to transgranular fracture, evidenced by river patterns (Fig. 4(f)).

While synthesizing the high-entropy carbide is relatively straightforward via UPS, achieving high density is more challenging. The timing of pressure application significantly influences densification. Applying pressure after the carbothermal reaction resulted in lower density (Fig. 5(a)), while applying pressure before the reaction, although improving density, led to edge cracking (Fig. 5(b)). The optimal approach involved applying pressure concurrently with the carbothermal reduction, resulting in improved shape integrity and higher relative density (Fig. 5(c)). A detailed explanation of the influence of the pressurization timing on ceramic sintering is provided in the Supplementary Information. Further investigation using optical microscopy (Fig. S1) demonstrated a clear correlation between applied pressure and densification, with relative density increasing with pressure and reaching 99 % at 60 MPa (1800 °C, 3 min dwell time).

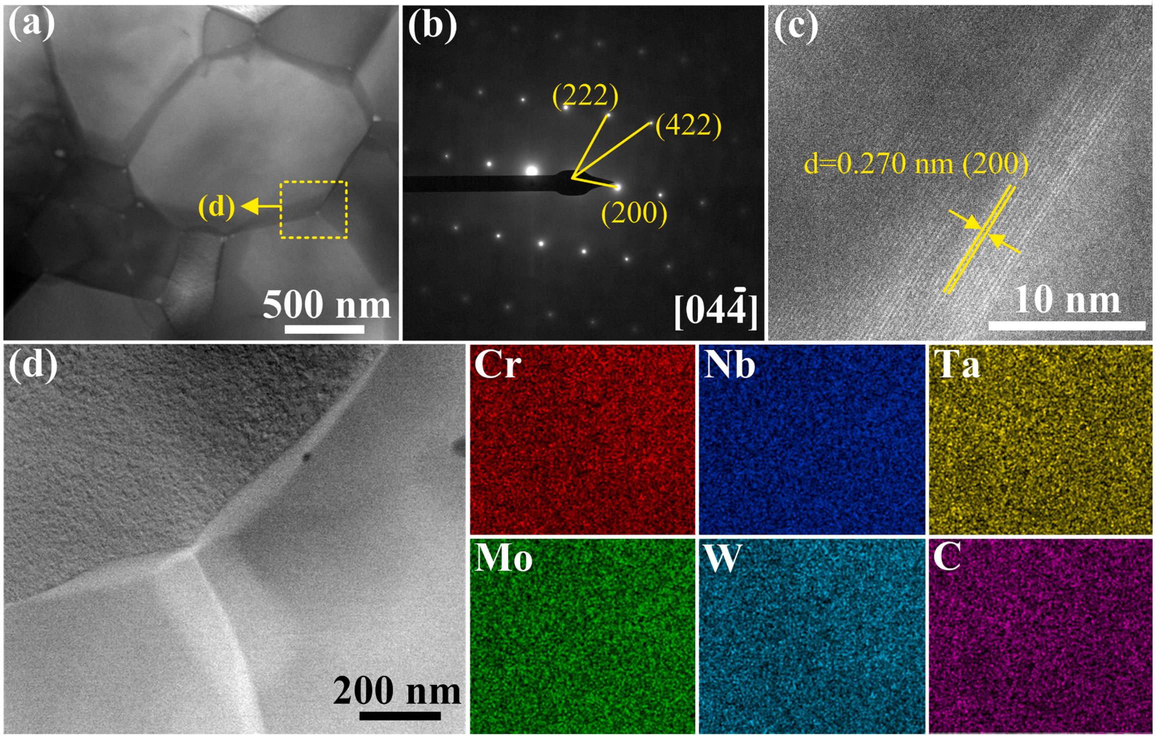

Fig. 6. Dense HEC sample processed at 1800 °C/60 MPa/3 min via UPS: (a) Bright-field TEM image; (b) Selected area electron diffraction pattern; (c) High-resolution TEM image; (d) Triple junction microstructure and elemental mappings.

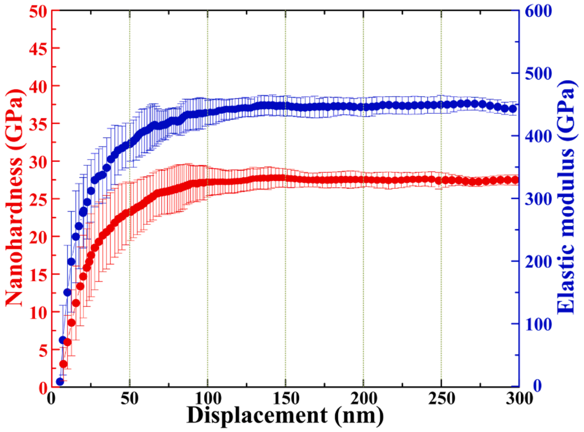

Fig. 7. Nanohardness- and elastic modulus-displacement curves of a dense sample prepared by UPS.

SEM and EDS analyses of this sample (Fig. 5(d)) revealed a uniform elemental distribution and an average grain size of approximately 2.5 µm. The measured carbon stoichiometry in the high-entropy carbide ceramic was 0.83 (Table S3). Given the relatively high volatility of WO_3 and MoO_2 at elevated temperatures, elemental quantitative analysis was performed on different areas of the dense ceramic to assess the potential loss of Mo and W. The elemental scanning results (Fig. S4) indicate that Mo and W concentrations remain relatively consistent across the sample. This suggests that the rapid heating rate (~160 °C/min) provided by the graphite felt allows the carbothermal reduction reactions of WO_3 and MoO_2 to occur before substantial volatilization losses can take place, minimizing stoichiometric deviations in the final product.

To further confirm compositional homogeneity at the micro-scale, TEM analysis was performed (Fig. 6(a)), revealing tightly bonded grains. Selected area electron diffraction (SAED) (Fig. 6(b)) and high-resolution TEM (Fig. 6(c)) analyses confirmed the single-phase FCC rock-salt structure. EDS mapping (Fig. 6(d)) revealed a homogeneous distribution of Cr, Nb, Ta, Mo, and W at the nanoscale, without significant segregation or agglomeration. This confirms the successful fabrication of a dense, fine-grained $(Cr_{0.2}Nb_{0.2}Ta_{0.2}Mo_{0.2}W_{0.2})C_{0.83}$ HEC with

Table 1
Properties of high entropy carbide ceramics prepared under different sintering methods.

Ceramic	Sintering method	Temperature (°C)/Pressure (MPa)/ Time (min)	Relative Density (%)	Grain size (µm)	Vickers hardness (GPa)	Elastic modulus (GPa)	Ref.
$(Cr_{0.2}Nb_{0.2}Ta_{0.2}Mo_{0.2}W_{0.2})C_{0.83}$	RS[a]: UPS	1800/60/3	99.0	2.5	24.4	453	This work
(NbTaMoW)C	RS[a]: SPS	1800/30/20	97.3	9.0	21.4	–	[15]
(VNbTaMoW)C	RS[a]: SPS	1850/30/20	97.7	10.0	22.8	–	[16]
(VNbTaMoW)C	NRS[b]: SPS	1900/30/12	97.5	5.1	19.6	551	[17]
$(TiVNbMoW)C_{4.375}$	NRS[b]: SPS	2200/30/5	98.1	20.0	18.6	536	[18]
$(Hf_{0.2}Zr_{0.2}Ta_{0.2}Nb_{0.2}Ti_{0.2})C$	NRS[b]: SPS	2000/30/5	93.0	16.4	15.0	479	[19]
(HfNbTaTiZr)C	NRS[b]: HP	1900/32/60	99.3	1.2	24.4	–	[20]
$(Hf_{0.2}Zr_{0.2}Ta_{0.2}Nb_{0.2}Ti_{0.2})C$	NRS[b]: PS[c]	2200/–/120	96.6	7.0	17.2	439	[21]
(CrNbTaTiV)C	NRS[b]: UHS[d]	2215/–/2	99.7	5.0	24.6	476	[7]

[a]RS refers to reactive sintering. [b] NRS refers to non-reactive sintering. [c] PS refers to pressureless sintering. [d] UHS refers to ultrafast high-temperature sintering.

homogeneous composition via the UPS process at a relatively low temperature and short dwell time.

Fig. 7 shows the nanohardness and elastic modulus of the high-entropy carbide. Due to the indentation size effect, both nanohardness and modulus increase sharply at depths below 50 nm and stabilize above 100 nm. Therefore, representative values were derived from indentation depths between 100 and 300 nm. The dense sample exhibited a nanohardness of 27.4 GPa and an elastic modulus of 453 GPa.

For comparison, the sintering methods and mechanical properties of various high-entropy carbide ceramics are summarized in Table 1. Comparing reactive and non-reactive sintering reveals that reactive sintering generally requires lower temperatures. However, the formation of high-entropy carbides from binary carbide precursors necessitates higher temperatures due to the energy required for interdiffusion and lattice reconstruction. During reactive sintering (RS), the exothermic heat from the carbothermal reduction contributes to lower sintering temperatures, facilitating the synthesis of high-entropy carbides. The key advantages of UPS for preparing high-entropy carbides include low energy consumption, short processing times, and the use of simple apparatus (Fig. 1(a)). The power required to reach 1800 °C in the UPS process is 3000–4000 W (Fig. 1(c)), compared to 6000–8000 W for SPS [14]. Additionally, hot-pressing (HP) typically requires 30 min, whereas UPS achieves full densification in just 3 min, with the entire process from heating to cooling completed within 15 min. In view of properties, the Vickers hardness (9.8 N load) of the dense $(Cr_{0.2}Nb_{0.2}Ta_{0.2}Mo_{0.2}W_{0.2})C_{0.83}$ ceramic fabricated in this study (24.4 GPa) is comparable to or even surpasses that of similar materials prepared by SPS, HP, or pressureless sintering (PS) [16,20,21]. This excellent performance is attributed to the fine grain size and the rapid heating and cooling rates, which can induce beneficial residual stresses [22–24].

4. Conclusions

This study demonstrates a novel and efficient ultrafast pressure sintering (UPS) method for the one-step synthesis and densification of high-entropy carbide ceramics. Compared to traditional methods like HP and SPS, UPS offers significant advantages, including lower energy consumption, shorter processing time, and simpler equipment. The results highlight the critical role of pressure application timing during carbothermal reduction for achieving optimal densification. Detailed microstructural and compositional analyses confirms the formation of a homogeneous, single-phase high-entropy carbide with a fine-grained microstructure. This study provides valuable insights into the synthesis and densification of high-entropy ceramics and paves the way for their broader application in demanding environments.

CRediT authorship contribution statement

Xiang-Yu Bai: Writing – original draft, Investigation, Formal analysis, Data curation. **Yu Sun:** Investigation. **Zhi-Yuan Cheng:** Investigation. **Ping Shen:** Writing – review & editing, Writing – original draft, Supervision, Methodology, Funding acquisition, Conceptualization.

Declaration of Competing Interest

The authors declare that they have no known competing financial interests or personal relationships that could have appeared to influence the work reported in this paper.

Acknowledgment

This work is supported by the National Natural Science Foundation of China (No. 52372061).

Appendix A. Supporting information

Supplementary data associated with this article can be found in the online version at doi:10.1016/j.jeurceramsoc.2024.117095.

References

[1] E. Castle, T. Csanádi, S. Grasso, J. Dusza, M. Reece, Processing and properties of high-entropy ultra-high temperature carbides, Sci. Rep. 8 (2018) 8609.

[2] T.J. Harrington, J. Gild, P. Sarker, C. Toher, C.M. Rost, O.F. Dippo, C. McElfresh, K. Kaufmann, E. Marin, L. Borowski, P.E. Hopkins, J. Luo, S. Curtarolo, D. W. Brenner, K.S. Vecchio, Phase stability and mechanical properties of novel high entropy transition metal carbides, Acta Mater. 166 (2019) 271–280.

[3] A. Nisar, C. Zhang, B. Boesl, A. Agarwal, A perspective on challenges and opportunities in developing high entropy-ultra high temperature ceramics, Ceram. Int. 46 (2020) 25845–25853.

[4] K. Wang, L. Chen, C.G. Xu, W. Zhang, Z.G. Liu, Y.J. Wang, J.H. Ouyang, X. H. Zhang, Y.D. Fu, Y. Zhou, Microstructure and mechanical properties of (TiZrNbTaMo)C high-entropy ceramic, J. Mater. Sci. Technol. 39 (2020) 99–105.

[5] X.F. Wei, Y. Qin, J.X. Liu, F. Li, Y.C. Liang, G.J. Zhang, Gradient microstructure development and grain growth inhibition in high-entropy carbide ceramics prepared by reactive spark plasma sintering, J. Eur. Ceram. Soc. 40 (2020) 935–941.

[6] C. Wang, W. Ping, Q. Bai, H. Cui, R. Hensleigh, R. Wang, A.H. Brozena, Z. Xu, J. Dai, Y. Pei, C. Zheng, G. Pastel, J. Gao, X. Wang, H. Wang, J.C. Zhao, B. Yang, X. R. Zheng, J. Luo, Y. Mo, B. Dunn, L. Hu, A general method to synthesize and sinter bulk ceramics in seconds, Science 368 (2020) 521–526.

[7] H.R. Mao, E.T. Dong, S.B. Jin, X.M. Qiu, P. Shen, Ultrafast high-temperature synthesis and densification of high-entropy carbides, J. Eur. Ceram. Soc. 42 (2022) 4053–4065.

[8] R.F. Guo, H.R. Mao, P. Shen, Ultra-fast high-temperature synthesis and densification of high-entropy diborides and diboride-carbide ceramics, J. Eur. Ceram. Soc. 43 (2023) 5763–5773.

[9] T. Che, H.R. Mao, R.F. Guo, P. Shen, Ultrafast synthesis and pressureless densification of multicomponent nitride and carbonitride ceramics, Ceram. Int. 49 (2023) 31530–31538.

[10] Y. Sun, X.Y. Bai, R.F. Guo, P. Shen, Ultrafast pressure sintering of B_4C-based composites via direct Joule heating, J. Mater. Sci. Technol. 210 (2025) 188–194.

[11] H.O. Pierson, Handbook of refractory carbides and nitrides: properties, characteristics, processing and applications, William Andrew (1996).

[12] H. Matzke, Diffusion in carbides and nitrides: unsolved problems, Defect Diffus. Forum, Trans. Tech. Publ. 83 (1992) 111–130.

[13] X.G. Wang, J.X. Liu, Y.M. Kan, G.J. Zhang, Effect of solid solution formation on densification of hot-pressed ZrC ceramics with MC (M = V, Nb, and Ta) additions, J. Eur. Ceram. Soc. 32 (2012) 1795–1802.

[14] S. Grasso, T. Saunders, H. Porwal, B. Milsom, A. Tudball, M. Reece, Flash Spark plasma sintering (FSPS) of α and β SiC, J. Am. Ceram. Soc. 99 (2016) 1534–1543.

[15] D.Q. Liu, A.J. Zhang, J.G. Jia, J.H. Meng, Reaction synthesis and characterization of a new class high entropy carbide (NbTaMoW)C, Mater. Sci. Eng. A 804 (2021) 140520.

[16] D.Q. Liu, A.J. Zhang, J.G. Jia, J.H. Meng, B. Su, Phase evolution and properties of (VNbTaMoW)C high entropy carbide prepared by reaction synthesis, J. Eur. Ceram. Soc. 40 (2020) 2746–2751.

[17] H. Chen, Z. Wu, M. Liu, W. Hai, W. Sun, Synthesis, microstructure and mechanical properties of high-entropy $(VNbTaMoW)C_5$ ceramics, J. Eur. Ceram. Soc. 41 (2021) 7498–7506.

[18] J.C. Li, Y.C. Zhou, Y.F. Su, S.N. Chen, Q.A. Sun, H.Z. Fan, J.J. Song, L.T. Hu, Y. S. Zhang, Synthesis and mechanical and elevated temperature tribological properties of a novel high-entropy $(TiVNbMoW)C_{4.375}$ with carbon stoichiometry deviation, J. Adv. Ceram. 12 (2023) 242–257.

[19] X.L. Yan, L. Constantin, Y.F. Lu, J.F. Silvain, M. Nastasi, B. Cui, $(Hf_{0.2}Zr_{0.2}Ta_{0.2}Nb_{0.2}Ti_{0.2})C$ high-entropy ceramics with low thermal conductivity, J. Am. Ceram. Soc. 101 (2018) 4486–4491.

[20] L. Feng, W.G. Fahrenholtz, G.E. Hilmas, Low-temperature sintering of single-phase, high-entropy carbide ceramics, J. Am. Ceram. Soc. 102 (2019) 7217–7224.

[21] D. Yu, J. Yin, B. Zhang, X. Liu, M.J. Reece, W. Liu, Z. Huang, Pressureless sintering and properties of $(Hf_{0.2}Zr_{0.2}Ta_{0.2}Nb_{0.2}Ti_{0.2})C$ high-entropy ceramics: the effect of pyrolytic carbon, J. Eur. Ceram. Soc. 41 (2021) 3823–3831.

[22] O.L. Ighodaro, O.I. Okoli, Fracture toughness enhancement for alumina systems: a review, Int. J. Appl. Ceram. Technol. 5 (2008) 313–323.

[23] Y. Wan, J.H. Gong, Influence of TiC particle size on the load-independent hardness of Al_2O_3–TiC composites, Mater. Lett. 57 (2003) 3439–3443.

[24] D. Kovar, S.J. Bennison, M.J. Readey, Crack stability and strength variability in alumina ceramics with rising toughness-curve behavior, Acta Mater. 48 (2000) 565–578.